Radially sheared azimuthal flows and turbulent transport in a cylindrical helicon plasma device

G R Tynan[1], **M J Burin**[1], **C Holland**[1], **G Antar**[1] **and P H Diamond**[2]

[1] Department of Mechanical and Aerospace Engineering, University of California, San Diego, USA
[2] Department of Physics, University of California, San Diego, USA

Abstract

A radially sheared azimuthal flow is observed in a cylindrical helicon plasma device. The shear flow is roughly azimuthally symmetric and contains both time-stationary and slowly varying components. The turbulent radial particle flux is found to peak near the density gradient maximum and vanishes at the shear layer location. The shape of the radial plasma potential profile associated with the azimuthal $E \times B$ flow is predicted accurately by theory. The existence of the mean shear flow in a plasma with finite flow damping from ion–neutral collisions and no external momentum input implies the existence of radial angular momentum transport from the turbulent Reynolds-stress.

The spontaneous formation of sheared flows in toroidal plasma devices (Groebner *et al* 1990), which has been demonstrated to lead to reduced turbulent transport across the shear layer in tokamak devices (Tynan *et al* 1994, Moyer *et al* 1995), is associated with both the low-confinement mode (L-mode) to high-confinement mode (H-mode) (L–H) transition (Wagner *et al* 1982) that occurs in the edge plasma region, as well as with the formation of internal transport barriers (ITBs) in the hot central plasma of such fusion confinement devices (Bell *et al* 1998). Theory suggests that the turbulent Reynolds-stress may act as a trigger for the formation of such time-stationary sheared flows (Diamond *et al* 1994), which once formed, can act to reduce the rate of cross-field turbulent mixing. For a constant cross-field particle and/or heat flux, the mean density and/or temperature profiles then evolve into steeper gradients across the shear layer region. Linearly damped time-varying shear flows such as zonal flows (Hasegawa *et al* 1979) are thought to be driven by the turbulent Reynolds-stress which couples unstable small-scale turbulence to large-scale (i.e. non-viscous) damping. Examples of the latter include neutral friction (as in our experiment), collisions between trapped and untrapped populations (as in a torus) and topographic friction (in the case of geophysical flows). As a result, the saturation amplitude of turbulence can depend upon non-linear turbulence–shear flow interactions even in the absence of an L–H transition or ITB formation, as has been shown in numerical simulations of plasma turbulence (Lin *et al* 1998).

When viewed as a wave–wave interaction problem (Diamond *et al* 2000, Tynan *et al* 2001), the turbulence energy is viewed as being transferred via three-wave interactions from the turbulence scales into the shear flow scales, where it is then damped. Using such an approach, recent studies of the L–H transition in DIII-D (Moyer *et al* 2001, Tynan *et al* 2001) have provided evidence that is qualitatively consistent with the existence of Reynolds-stress-driven L–H transitions, and studies of time-stationary plasmas in DIII-D and in the H-1 torsatron (Shats and Solomon 2001, Jakubowski *et al* 2002) provide evidence that is consistent with the existence of turbulence-driven time-varying shear flows. However, we also note that recent numerical studies have cast some doubt upon the usefulness of the autobicoherence of potential fluctuations as a means of detecting turbulence-driven shear flows (Ramisch *et al* 2003). Theory indicates that such effects should also occur in simple experimental geometries (Hasegawa and Wakatani 1987) where the complications that arise in a toroidal geometry (e.g. a bifurcation in the neoclassical viscosity (Shaing and Crume 1989)) can be avoided. In this paper we report initial observations of a radially varying plasma potential profile (which signals the existence of a velocity shear layer) at the edge of a region of collisional drift turbulence in a cylindrical helicon plasma device. The shear layer contains both time-stationary and time-varying components, and the turbulent particle flux across the shear layer vanishes.

The experiments were performed in the Controlled Shear Decorrelation eXperimental (CSDX) plasma device, which is a cylindrical plasma device that uses an azimuthally symmetric ($m = 0$) helicon wave antenna to generate a dense ($\sim 10^{19}\,\mathrm{m}^{-3}$) cold ($T_{\mathrm{e}} \sim 3\,\mathrm{eV}$, $T_{\mathrm{i}} \sim 0.2$–$0.8\,\mathrm{eV}$) plasma immersed within a solenoidal magnetic field that can be varied from 0 up to 1000 G. The plasma source is 10 cm in diameter, and the vacuum chamber has an inside diameter of 20 cm. For all these experiments argon plasmas were used with a fill pressure of 3 mTorr, a magnetic field of 1000 G, and an RF source power of 1500 W at a frequency of 13.56 MHz (usually less than 50 W was reflected, and measurements of the antenna current, voltage, and phase under conditions similar to these experiments indicate that greater than 80% of the RF power is absorbed in the plasma itself). In the plasma source region the magnetic field lines terminate on insulating surfaces, while at a distance 1.9 m downstream from the exit plane of the plasma source (defined as $z = 0\,\mathrm{m}$) the magnetic field lines terminate on a series of ten conducting annular rings. Each ring has a radial extent of about 3 mm and is separated from the next ring by a gap of about 2 mm (a distance that is of the order of an ion gyroradius, estimated to be 2–4 mm at these conditions). In all the experiments reported here the end rings were electrically isolated from each other and from the grounded chamber, inhibiting the radial transport of current between rings. Thus, any radial currents must occur within the plasma via polarization drifts or other non-ambipolar transport mechanisms (which have been shown to be equivalent to a Reynolds-stress effect (Diamond and Kim 1991)). Measurements of the equilibrium plasma conditions were made at $z = 1.2\,\mathrm{m}$ with a RF-compensated swept probe (Sudit and Chen 1994) that could be scanned across the plasma column. Measurements of the fluctuating ion saturation current and floating potential were also made at $z = 1.2\,\mathrm{m}$ with a four-tip probe assembly that had two Isat probe tips, azimuthally separated by 0.5 cm, both aligned along the field line with two floating probe tips that were also separated azimuthally by 0.5 cm. Comparisons of the low-frequency ($\omega < \Omega_{\mathrm{ci}}$, where Ω_{ci} is the ion cyclotron frequency) floating potential fluctuations made with and without RF compensation indicated no substantive difference between the measured spectra, suggesting the RF fluctuations are not affecting the low-frequency potential fluctuation measurements. Details of the RF antenna design and source operation in a divergent magnetic field have been given previously (Tynan 1997). Details of the CSDX device geometry, diagnostic layouts, and biasing ring assembly are also available (George 2002, Burin 2003).
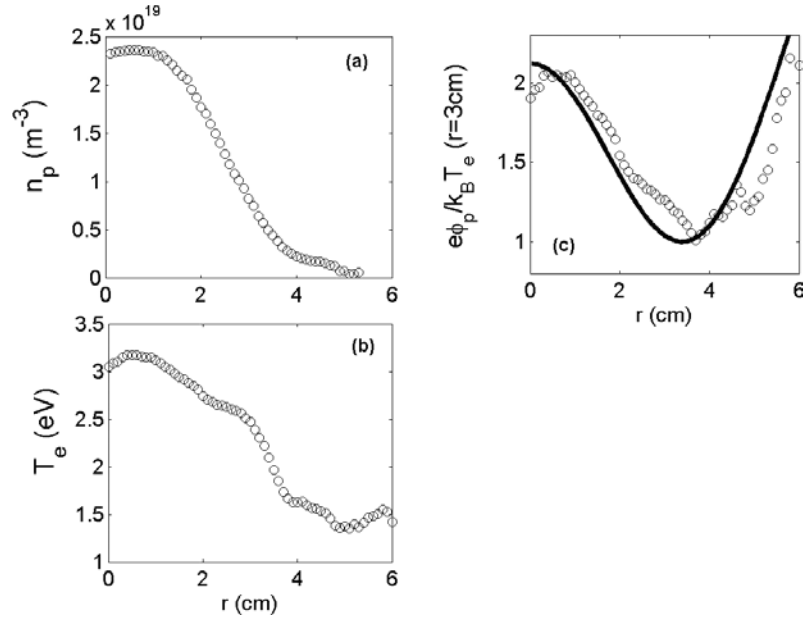
Figure 1. Time-averaged radial profiles of (a) plasma density, (b) electron temperature, and (c) measured ($\bigcirc$) and predicted (——) plasma potential. In (c), the plasma potential is normalized to the electron temperature measured at $r = 3$ cm. $P_{RF} = 1.5$ kW, $P_{gas} = 3.0$ mTorr, argon flow rate $= 14.7$ sccm, $B = 1000$ G.

The measured equilibrium density and electron temperature are shown in figures 1(a) and (b), respectively. The central plasma density is about 2.4×10^{19} m^{-3} and has roughly a Gaussian profile shape. The temperature profile peaks in the centre of the plasma and has a slow decay with increasing radius for $r < 3$ cm. At larger radii the electron temperature decreases more quickly, consistent with the plasma source acting as a heat source localized in the inner few centimetres of the plasma column. The minimum density gradient scale length, $L_n \equiv n(\partial n/\partial r) \approx 2$ cm, occurs at $r = 3$ cm for these conditions, about twice the value of the modified ion gyroradius, $\rho_s \equiv C_s/\Omega_{ci} \approx 1$ cm (here C_s is the ion acoustic speed); the electron temperature gradient scale length, $L_T \equiv T_e/(\partial T_e/\partial r) \approx 2$–3 cm at $r = 3$ cm, indicating that the pressure gradient contains contributions from both temperature and density gradients. Under these conditions, parallel electron motion is inhibited primarily by electron–ion Coulomb collisions (we estimate that electrons make about ten small-angle ion collisions during a transit along the axis of the device) and thus collisional drift waves can be unstable in this plasma, provided the magnetic field is strong enough (Burin 2003a). The ion–neutral collision frequency is about four-times smaller than the ion gyrofrequency, providing a damping mechanism for plasma flows, and the ion–ion collision frequency $\nu_{ii} \approx (1$–5$) \times \Omega_{ci}$, depending upon T_i (and thus collisional effects such as Petersen currents might also be important in this experiment). The measured plasma potential profile, normalized to the value of T_e at $r = 3$ cm, is shown as open circles in figure 1(c). The plasma potential peaks at the centre of the plasma, has a minimum at $r = 4$ cm, and then begins to increase for $r > 4$ cm. Thus a positive radial electric field exists in the inner portion of the plasma column and a negative electric field exists outside of a shear layer located at $r \approx 4$ cm near the potential minimum.

Using arguments based upon the conservation of angular momentum, the shape of the time-averaged plasma potential profile associated with a radially sheared azimuthal $E \times B$
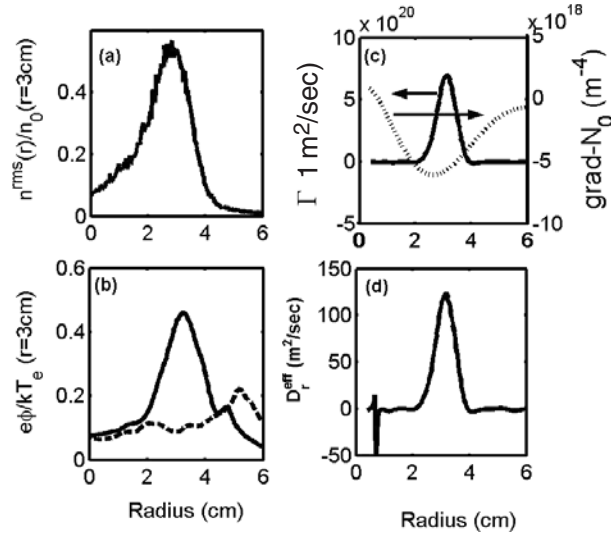
Figure 2. Radial profiles of (*a*) normalized broadband plasma density fluctuations, $\tilde{n}/n_0$, and (*b*) floating potential fluctuations, $e\tilde{\phi}/kT_e$ (broadband fluctuations indicated by solid line; low-frequency, low-$k_\theta \rho_s$ fluctuations indicated by dashed line). (*c*) Turbulent cross-field particle flux $\tilde{\Gamma}_r = \langle \tilde{n}\tilde{v}_r \rangle$ (——) and equilibrium density gradient, ∇n_0 (- - - -), and (*d*) effective radial particle diffusivity $D_r^{\mathrm{eff}} = -\tilde{\Gamma}_r/\nabla n_0$. Data cover frequency range $\omega \leqslant \Omega_{\mathrm{ci}}$. In panels (*a*) and (*b*), the data were normalized by the equilibrium values at $r = 3$ cm. $P_{\mathrm{RF}} = 1.5$ kW, $P_{\mathrm{gas}} = 3.0$ mTorr, argon flow rate = 14.7 sccm, $B = 1000$ G.

flow formed via an inverse energy transfer process was predicted theoretically (Hasegawa and Wakatani 1987). In this theory, the radial transport of turbulent angular momentum via the turbulent Reynolds-stress, or equivalently a non-linear transfer of turbulence kinetic energy to large azimuthal scales, leads to the build-up of two regions of oppositely directed azimuthal flow, which results in the formation of a shear layer that conserves angular momentum. The theory also assumes that the electron temperature is uniform and that the plasma density has a form $n(r) = n_0[0.9 \exp(-2r^2/a^2) + 0.1]$, where the radius a defines the size of the plasma in the simulations. The density profile shown in figure 1(*a*) is reasonably close to this form for $a \approx 3.8$ cm. Using this value to scale the system size with the theoretical predicted potential profile, we find that the predicted potential profile agrees well with the measured space potential profile (see solid line in figure 1(*c*)). The theory does not provide an absolute magnitude for the peak plasma potential, and thus the peak-to-peak magnitude of the predicted potential was normalized to the experimental measurements. Thus, the only meaningful observation to make at this point is to point out the excellent agreement between the shape of the predicted potential profile (i.e. the relative shear rate) and the shape of the experimental measurements.

The radial profiles of the low-frequency (i.e. $\omega < \Omega_{\mathrm{ci}}$) plasma density and electrostatic potential fluctuations are shown in figures 2(*a*) and (*b*). The solid lines in these panels indicate the rms amplitude of the broadband fluctuations normalized to the equilibrium values of density and electron temperature at $r = 3$ cm. As will be reported elsewhere (Burin *et al* 2004), the density and potential fluctuations are a mixture of broadband collisional drift turbulence localized to the density gradient region with a low-order ($m = 3$–5) chain of coherent structures of vortices centred about the shear layer. The potential fluctuations also have a low-frequency (<2 kHz) component with peak amplitude at $r \approx 5$ cm located just outside the minimum in the time-averaged potential profile (as shown by the dashed line in figure 2(*b*)) and located roughly at the edge of the gradient in the broadband fluctuation amplitudes.
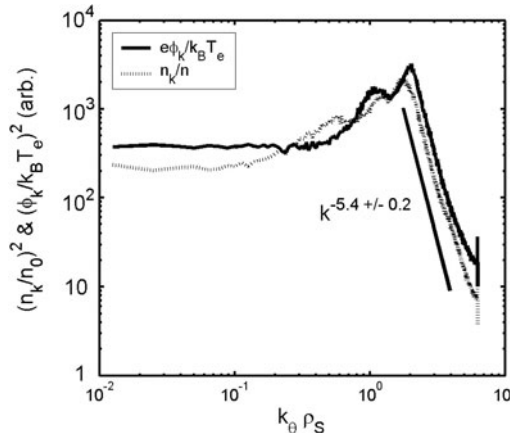
Figure 3. Local azimuthal wavenumber spectra of density and potential fluctuations. Measurements obtained at $r = 3$ cm near the density gradient maximum. The local wavenumber is defined in the text. $P_{RF} = 1.5$ kW, $P_{gas} = 3.0$ mTorr, argon flow rate $= 14.7$ sccm, $B = 1000$ G.

The density and potential fluctuations were both simultaneously measured at two azimuthal locations separated by 0.5 cm in order to permit the measurement of the local azimuthal wavenumber spectra, $S(k_\theta)$, using established techniques (Beall *et al* 1982) (note that here the local wavenumber is defined as the rate of change of the phase, ϕ, of a fluctuation with respect to the change in position, x, i.e. $k = \delta\phi/\delta x$). The measured density and potential local wavenumber spectra, $S_{nn}(k_\theta)$ and $S_{\phi\phi}(k_\theta)$, are shown in figure 3 for $r = 3$ cm. The spectra peak at an intermediate wavenumber, $k_\theta\rho_s \sim 2$, and decay as $\sim k_{\theta s}^{-5.4\pm0.2}$ for higher wavenumbers. Interestingly the low-wavenumber portion of the potential spectrum, $k_\theta\rho_s < 0.5$, which corresponds to the low-frequency region below 2 kHz, appears to have appreciable amounts of power (i.e. significantly higher than the noise level of the measurement) and contains about twice the power contained in the low-wavenumber density fluctuations. The mean wavenumber of the potential fluctuations at $r = 4$–5 cm is $k_\theta \approx 0.1$ cm^{-1} and has a variation $\delta k_\theta \approx 0.3$ cm^{-1} centred about this mean. Thus the low-frequency fluctuation corresponds to an $m \approx 0$ azimuthally symmetric potential fluctuation that modulates the strength of the mean shear flow associated with the radial plasma potential profile shown in figure 1(*c*). This shear flow modulation also contains significant finite k_θ components, indicating that the fluctuating shear flow also contains finite azimuthal wavelength perturbations.

Given the existence of both a mean and fluctuating azimuthal shear flow, one is naturally tempted to infer that this is, in fact, a zonal flow. Caution must be used at this point in time when making such an inference because, for example, we note that the density fluctuation power at $k_\theta\rho_s < 0.5$ is also significant. If the fluctuating shear flow is indeed a turbulence-driven zonal flow, then this result is surprising since theory suggests that, at least in collisionless toroidal devices, zonal flows should not exhibit a significant density fluctuation component (Diamond *et al* 2000). Our experiment does show such fluctuation components, but our experiment also has finite collision frequencies and boundary conditions, and/or finite parallel wavenumber effects may also allow a finite density fluctuation with $k_\theta\rho_s \ll 1$ (Horton 1999). We have also not addressed the non-linear coupling between the shear flow and the turbulence in this paper—a key requirement for zonal flows. We do note, however, that the fact that a mean flow still exists without any external torque input despite the presence of flow dissipation implies that stochastic turbulent angular momentum must be transported radially in such a way as to maintain the shear flow. Such radial transport of turbulent angular momentum is caused by

the Reynolds-stress. Thus, the results observed here seem to us to imply at least the presence of a turbulent Reynolds-stress that maintains the observed shear flow.

The broadband density and potential fluctuations have a decorrelation rate $\nu_{corr} \sim \Delta\omega \sim 6 \times 10^4 \, s^{-1}$, where $\Delta\omega$ is the width of the measured frequency spectrum near the shear layer, where Doppler shifts are small. The shearing rate due to the mean shear flow (Biglari *et al* 1990) is $\omega_{sh} = k_\theta (\partial V_E / \partial r) L_r^{corr}$ where V_E is the $E \times B$ drift speed. As shown in figure 3, we find that the peak fluctuation power occurs for an azimuthal wavenumber $k_\theta \approx 2 \, cm^{-1}$, and from figure 1(*c*) we estimate that $\partial V_E / \partial r \approx 10^5 \, s^{-1}$. If the radial correlation length $L_r^{corr} \approx L_n = 2 \, cm$, then we estimate that $\omega_{sh} \approx 4 \times 10^5 \, s^{-1}$. The hybrid decorrelation rate $(2\omega_{sh}^2 \nu_{corr})^{1/3} \approx (2-3) \times 10^5 \, s^{-1}$, which gives the net effective decorrelation rate of the turbulence in the presence of the shear flow (Biglari *et al* 1990), is thus a few times higher than ν_{corr}. As a result, the shear flow might be expected to affect the turbulence according to the usual shear decorrelation arguments. The radial profile of the time-averaged turbulence particle flux $\Gamma_r = \langle \tilde{n} \tilde{E}_\theta \rangle / B$ inferred from the measured density and electric field fluctuations and the equilibrium density gradient, ∇n_0, are shown as solid and dashed lines in figure 2(*c*), respectively. The turbulent particle flux peaks near $r = 3 \, cm$, where ∇n_0 reaches a maximum, and then goes to zero close to the position of the shear layer, as might be expected from the shear decorrelation arguments discussed above and as also shown in numerical simulations (Hasegawa and Wakatani 1987). An effective diffusivity can be defined from these quantities as $D_r^{eff} \equiv -\Gamma_r / \nabla n_0$ and is shown in figure 2(*d*). The particle diffusivity peaks near $r = 3 \, cm$ and vanishes near the machine axis (where ∇n_0 essentially goes to zero) as well as at $r = 4 \, cm$, where the velocity shear layer is located (and also where $|\nabla n_0|$ has fallen to about half the peak value). The particle flux and effective diffusivity thus both vanish at the position of the shear layer, and at the same time, the density gradient falls by a factor of 2. These observations suggest that the shear layer may play a role in the transport reduction but also suggest that changes in transport due to changes in the local gradient may also be important.

In summary, we report evidence for the formation of a velocity shear layer that exists at the edge of a region of collisional drift turbulence in a cylindrical helicon plasma device. This shear flow contains both a time-stationary mean component as well as a low-frequency fluctuating component. The density and potential, k_θ, spectra have both been measured and show that the large azimuthal scale lengths contain significant fluctuation power. The time-averaged potential profile, which represents the mean azimuthal $E \times B$ flow, is in good agreement with theoretical predictions (Hasegawa and Wakatani 1987). The turbulent particle flux vanishes at the position of the shear layer, suggesting a causal relationship between the two quantities. However, simultaneous changes in the density profile prevent us from drawing a firm correlation between shear layer activity and transport reduction at this point in time. The existence of such a steady-state shear layer in a plasma with no external torque inputs and finite flow damping implies the existence of a turbulent Reynolds-stress that transports turbulent angular momentum radially in such a way as to maintain the organized shear flow. Work is under way to measure directly the Reynolds-stress and non-linear energy transfer in this experiment and will be reported in future work.

References

Beall J M, Kim Y C and Powers E J 1982 *J. Appl. Phys.* **53** 3933–40
Bell R E *et al* 1998 *Plasma Phys. Control. Fusion* **40** 609–13
Biglari H, Diamond P H and Terry P W 1990 *Phys. Fluids-B Plasma Phys.* **2** 1
Burin M J 2003 Structure formation and the transition to turbulence in a magnetized plasma column *PhD Dissertation* Department of Mechanical and Aerospace Engineering, UC San Diego
Burin M B, Tynan G R, Antar G and Holland C 2004 *Phys. Plasmas* to be submitted

Diamond P H and Kim Y-B 1991 *Phys. Fluids-B Plasma Phys.* **3** 1626–33

Diamond P H, Liang Y-M, Carreras B A and Terry P W 1994 *Phys. Rev. Lett.* **72** 2565–8

Diamond P H *et al* 2000 *Phys. Rev. Lett.* **84** 4842–5

George J 2002 Experimental study of linear resistive drift waves in a helicon plasma device *MS Thesis* Department of Mechanical and Aerospace Engineering, UC San Diego

Groebner R J, Burrell K H and Seraydarian R P 1990 *Phys. Rev. Lett.* **64** 3015–18

Hasegawa A, Maclennan C G and Kodama Y 1979 *Phys. Fluids* **22** 2122–9

Hasegawa A and Wakatani M 1987 *Phys. Rev. Lett.* **59** 1581–4

Horton W 1999 *Rev. Mod. Phys.* **71** 735

Lin Z *et al* 1998 *Science* **281** 1835–7

Jakubowski M, Fonck R J and McKee G R 2002 *Phys. Rev. Lett.* **89** 265003/1–4

Moyer R A *et al* 1995 *Phys. Plasmas* **2** 2397–407

Moyer R A, Tynan G R, Holland C and Burin M J 2001 *Phys. Rev. Lett.* **87** 135001/1–4

Ramisch M, Stroth U, Niedner S and Scott B 2003 *New J. Phys.* **5** 12.1–11

Shaing K C and Crume E C Jr 1989 *Phys. Rev. Lett.* **63** 2369–72

Shats M G and Solomon W M 2001 *Phys. Rev. Lett.* **88** 045001–4

Sudit I D and Chen F F 1994 *Plasma Sources Sci. Technol.* **3** 162–8

Tynan G R, Moyer R A, Burin M J and Holland C 2001 *Phys. Plasmas* **8** 2691–9

Tynan G R *et al* 1994 *Phys. Plasmas* **1** 3301–7

Tynan G R *et al* 1997 *J. Vac. Sci. Technol.* A **15** 2885–92

Wagner F *et al* 1982 *Phys. Rev. Lett.* **49** 1408–12